IEEE Access
Multidisciplinary | Rapid Review | Open Access Journal

Received August 4, 2019, accepted August 21, 2019, date of publication August 28, 2019, date of current version September 13, 2019.

Digital Object Identifier 10.1109/ACCESS.2019.2938064

Adsorption of SF_6 Decomposition Components on Pt-Doped Graphyne Monolayer: A DFT Study

YINGANG GUI, XIN HE, ZHUYU DING, CHAO TANG, AND LINGNA XU
College of Engineering and Technology, Southwest University, Chongqing 400715, China

Corresponding author: Yingang Gui (yinganggui@swu.edu.cn)

This work was supported in part by the National Natural Science Foundation of China under Grant 51907165, in part by the Chongqing Research Program of Basic Research and Frontier Technology under Grant cstc2018jcyjAX0068, and in part by the Fundamental Research Funds for the Central Universities under Grant SWU118030.

ABSTRACT To propose a novel type of sensing material applied in the field of sulfur hexafluoride (SF_6) insulated gas, we investigated the adsorption performance of SF_6 decomposed species (H_2S, SO_2, and SOF_2) on Pt-doped graphyne (GD) monolayer. We initially studied the possible stable structure of Pt–GD monolayer and found that the Pt dopant preferred adsorption onto the C≡C bond. We further investigated electronic differential density, band structure, and density of states to evaluate the chemical and physical interactions between Pt–GD and four typical gases, namely, H_2S, SO_2, SOF_2, and SF_6. The results indicated that only H_2S, SO_2, and SOF_2 molecules were adsorbed onto the Pt–GD with strong chemical interactions due to the large adsorption energy, evident electronic differential density change, and orbital hybridization. These results showed that the strong interactions were caused by the Pt dopant. The conductivity of monolayer was enhanced by H_2S but was weakened by SO_2 and SOF_2. The adsorption capacity occurred in the following order: $SO_2 > H_2S > SOF_2 > SF_6$. Our work determined the stable Pt doping structure on GD and provided theoretical support for a novel material realizing the operation state evaluation of SF_6 insulated gas equipment.

INDEX TERMS SF_6 decomposition components, Pt–doped graphyne, surface adsorption, DFT.

I. INTRODUCTION

Sulfur hexafluoride (SF_6) gas is widely used in high-voltage power equipment, such as gas-insulated switchgear, gas-insulated breaker, and gas-insulated metal enclosed transmission line on account of its excellent insulation performance, arc extinguishing performance, and stable chemical properties [1], [2]. In virtue of partial discharge, arc, and park, SF_6 gas molecule will decompose into SF_4 and F^-, which will regenerate SF_6 molecule in the absence of gas impurity [3], [4]. In the presence of trace amounts of air and water vapor, SF_4 molecules react as follows: $SF_4 + H_2O = SOF_2 + 2HF$, $SOF_2 + H_2O = SO_2 + HF$. A series of reactions is also involved. SF_6 decomposition end products include H_2S, SO_2, SOF_2, SO_2F_2, and HF [2], [3], [5], [6]. Gas impurity deteriorates the insulation property of SF_6, and a gas sensor is an efficient means to ensure equipment operation by monitoring decomposition products [7].

The associate editor coordinating the review of this article and approving it for publication was Huamin Li.

Graphyne (GD) is the first new carbon allotrope formed by the hybridization of sp, sp^2, and sp^3 and is the most likely carbon allotrope to be synthesized artificially [8]–[10]. GD has abundant carbon chemical bonds and excellent chemical stability and semiconductor properties. GD and its compound material exhibit good properties for application in various fields [11]–[15]. In the application of GD as a gas sensor, V. Nagarajan found that boron-substituted GD nanosheet is a good material to detect dimethyl amine and trimethyl amine molecules and investigated the adsorption behavior of ammonia; zigzag GD nanosheet is found to be a promising gas sensing material [16], [17]. GD is a novel material for the efficient monitoring of amino acid and adsorption of harmful gases from oxygen. However, the response of intrinsic GD to H_2S and SO_2 is insensitive [7], [18]–[22]. Metal atoms have been doped to improve the sensitivity of intrinsic materials.

Xi Chen et al. showed that in GD doped with Sc, Ti atoms are stable at room temperature and can adsorb HCHO efficiently [23]. Ali AhmadiPeyghan et al. studied the adsorption of NH_3 on pristine and Ni- and Si-doped GD and found

This work is licensed under a Creative Commons Attribution 4.0 License. For more information, see http://creativecommons.org/licenses/by/4.0/

TABLE 1. Information on PT–GD structures.

Structure	Fig.1 (a)	Fig.1 (b)	Fig.1 (c)	Fig.1 (d)	Fig.1 (e)	Fig.1 (f)	Fig.1 (g)	Fig.1(h)
E_{ads} (eV)	10.68	10.12	-1.55	-1.67	-1.67	-1.53	-1.67	-1.67
Q (e)	0.38	0.32	0.24	0.15	0.15	0.20	0.15	0.15

that the NH_3 molecule shows strong interactions with the Ni- and Si-doped GD [24]. When the adsorption of HCN on the pristine and Si-doped GD is compared, the GD monolayer shows increased sensitive to HCN gas after Si atom doping [25]. Considering the excellent gas adsorption and sensing properties of metal-modified GD [26]–[28], this work investigated the adsorption and sensing mechanism of Pt-doped GD monolayer upon SF_6 and its decomposition products (H_2S, SO_2, SOF_2) by determining the total density of states (TDOS), partial density of states (PDOS), band structure, and adsorption energy data based on the density functional theory (DFT) calculations [29].

II. COMPUTATION DETAILS

In this work, all calculations were performed based on DFT. The generalized gradient approximation with the Perdew-Burke-Ernzerhof (GGA-PBE) function which considers the variation of electron density gradient was chosen to calculate geometry optimization and energy [30]. However, Dispersion correction is absent for GGA, we carried out TS method to correct long-range dispersion energy to rectify van der Waals force. Energy convergence accuracy, max force, and max displacement were set to 10^{-5} Ha, 2×10^{-3} Ha/Å, and 5×10^{-3} Å, respectively. Regardless of the effect of spin polarization, we selected double numerical plus polarization as the basis set. Self-consistent field convergence accuracy was set to 10^{-6} Ha, and the DIIS field was set to 6 to accelerate convergence. We carried out a Monkhorst-Pack grid of $5\times5\times1$ to perform Brillouin zone integrations and set the Monkhorst-Pack grid to $10\times10\times1$ when the density of states (DOS) were calculated [27], [28], [31], [32]. All charge quantities in this paper refer to the Mulliken atomic charge. We built a 2×2 single-layer GD supercell with 15 Å vacuum slab to avert interaction between layers.

The adsorption energy (E_{ads}), charge transfer (Q_{tran}), and energy gap (E_{gap}) were calculated using (1), (2), and (3):

$$E_{ads} = E_{Pt-GD/gas} - E_{Pt-GD} - E_{gas} \quad (1)$$

$$Q_{tran} = Q_{ads} - Q_{iso} \quad (2)$$

$$E_{gap} = |E_{HOMO} - E_{LUMO}| \quad (3)$$

where $E_{Pt-GD/gas}$ is the total system energy after Pt-GD adsorbing gas, and E_{Pt-GD} and E_{gas} are the energy of insolated doping monolayer and gas molecule, respectively. Q_{ads} and Q_{iso} denote the charge amount of gas molecule before and after adsorption, respectively. The value of Q_{iso} was always 0 e in this work, and Q_{ads} was calculated by electron population analysis. A negative Q_{tran} indicates electron transfer from the Pt–GD monolayer to gas molecule.

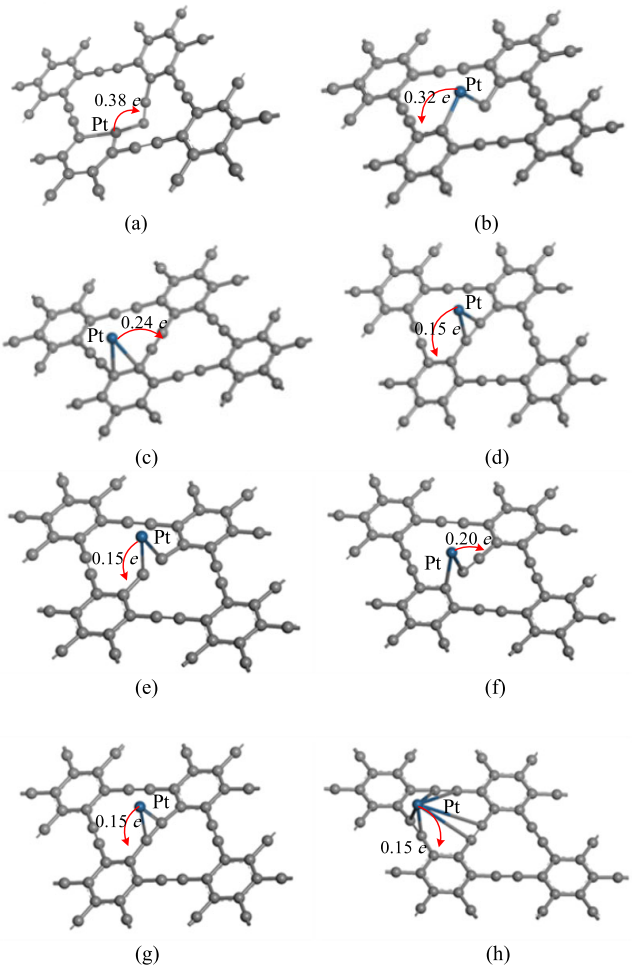

FIGURE 1. Eight types of Pt-GD structures.

E_{HOMO} and E_{LUMO} denote the energy of the highest and lowest unoccupied molecular orbitals, respectively.

III. RESULTS AND DISCUSSION

A. SELECTION OF THE PT-DOPED STRUCTURE

Fig. 1 shows eight types of Pt–GD structures and marks the charge transfer after geometry optimization, and its binding energy is shown in Table 1. The large binding energy of structures in Fig. 1(a) and (b) indicates that the doping process needs to adsorb a large amount of energy, which is unstable. Binding energy was −1.67 eV in the structures shown in Fig. 1(d), (e), (g), and (h) but was −1.55 eV in those presented in Fig. 1(c) and (f), indicating instability because of the less energy released compared with that of the structures in Fig. 1(d), (e), (g), and (h) during the doping procedure.

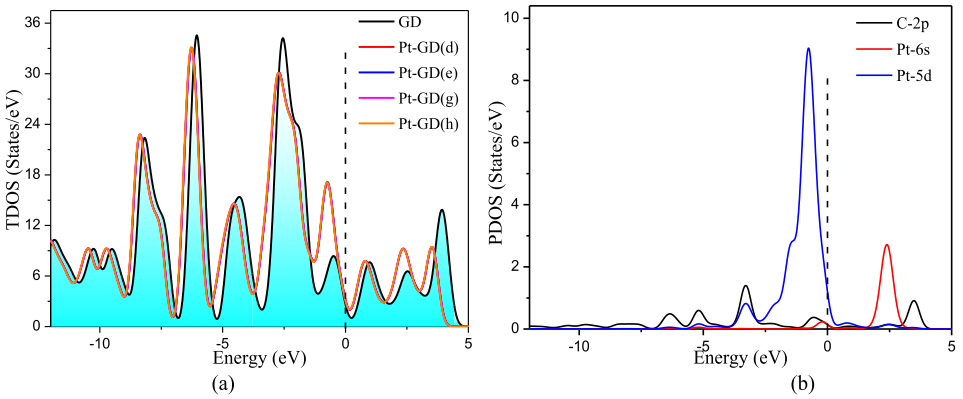

FIGURE 2. (a) Total density of states of GD and Pt–GD structures, (b) partial density of states of Pt and C atoms.

The structures in Fig. 1(d), (e), (g), and (h) show that the Pt dopant preferred adsorption and stabilization onto C≡C bond. The rich charges and strong reducibility of Pt resulted in abundant electrons transferred from Pt to GD surface.

Fig. 2(a) shows the TDOS of intrinsic GD monolayer and Pt–GD structures in Fig. 1(d), (e), (g), and (h), where the dash represents the Fermi level. The TDOS of Pt–GD completely overlapped, and its left-shift curve was more stable than that of the intrinsic GD monolayer because additional states moved toward low energy levels. Compared with that of the intrinsic GD monolayer, the TDOS of Pt–GD remarkably increased near the Fermi level, the reason for which is presented in Figure 2(b). The Pt-5d and Pt-6s orbitals remarkably contributed to the increase of TDOS and Pt-5d hybridization with C-2p at −3.3eV. Slight hybridization occurred between C-2p and Pt-6s around the Fermi level. Furthermore, we listed the energy gap (E_{gap}) of intrinsic GD monolayer and Pt–GD monolayer in accordance with (3) in Table 2 with band gap.

Given the same TDOS, adsorption energy (−1.67 eV), amount of charge (0.15 e), and band gap (0.24 eV), the four Pt-GD structures were apparently the same structures. Therefore, we only further investigated the structure in Fig. 1 (e).

The decreased band gap and remarkably increased DOS near the Fermi level implied high conductivity, which was consistent with the strong conductivity of Pt metal. In summary, these results indicated the presence of orbital hybridization between Pt dopant and the attached C atoms. According to the E_{ads} (−1.67 eV), charge transfer (0.15 e), and TDOS after doping, a strong reaction between Pt atom and GD monolayer occurred, and the binding was stable.

B. ADSORPTION AND GAS SENSITIVITY UPON H_2S

We calculated adsorption by placing the H_2S molecule at diverse initial adsorption sites to search for stable adsorption site, and the results are shown in Fig. 3 and Table 3. An 'H' 'initial position' column in Table 3 indicates that the H atom at the inner H_2S molecule was initially close to Pt–GD. Our research indicates that even if the H_2S molecule was placed

TABLE 2. Band gap and E_{gap} of GD and PT–GD.

Configuration	E_{HOMO} (eV)	E_{LUMO} (eV)	Band gap (eV)	E_{gap} (eV)
GD	-5.37	-4.95	0.44	0.42
Fig.1 (d)	-5.20	-4.98	0.24	0.22
Fig.1 (e)	-5.20	-4.98	0.24	0.22
Fig.1 (g)	-5.20	-4.98	0.24	0.22
Fig.1 (h)	-5.20	-4.98	0.23	0.22

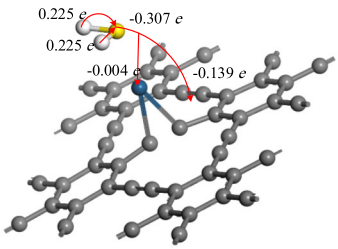

FIGURE 3. Adsorption position of H_2S gas molecule.

at diverse initial sites, Pt–GD could only strongly adsorb the S atom. The adsorption energy between Pt–GD and H2S molecule was −1.08 eV (< −0.6 eV) with the adsorption distance of 2.46 Å, implying strong chemisorption between Pt–GD and H_2S. The amount of charge transfer was a positive number (0.14 e), indicating electron transfers from the H_2S molecule to the Pt–GD. As shown in Fig. 3, the H atoms of H_2S were charge contributors, and the S atom accumulated a large charge. The GD substrate received most of the remaining charge, whereas Pt received minimal charge. This finding appears to be the electrostatic effect of positively charged Pt atoms on H_2S.

We further investigated orbital hybridization to reveal the adsorption mechanism. Considering that the outer electron orbits contributed to the reaction between atoms, the outer electron orbitals of Pt and S atoms are marked in Fig. 4. Strong chemisorption caused by the S-3p and Pt-5d orbitals occurred at the range of −4.5 eV to −2.5 eV. The electron differential density map after adsorption is shown in Fig.4 (b), unless otherwise specified, and the increase and decrease

TABLE 3. Adsorption data of H_2S gas molecule.

Initial position	E_{ads} (eV)	$d_{Pt\text{-}S}$ (Å)	Q_{trans} (e)	E_{gap} (eV)
H	-1.06	2.46	0.15	0.19
S	-1.08	2.46	0.14	0.15

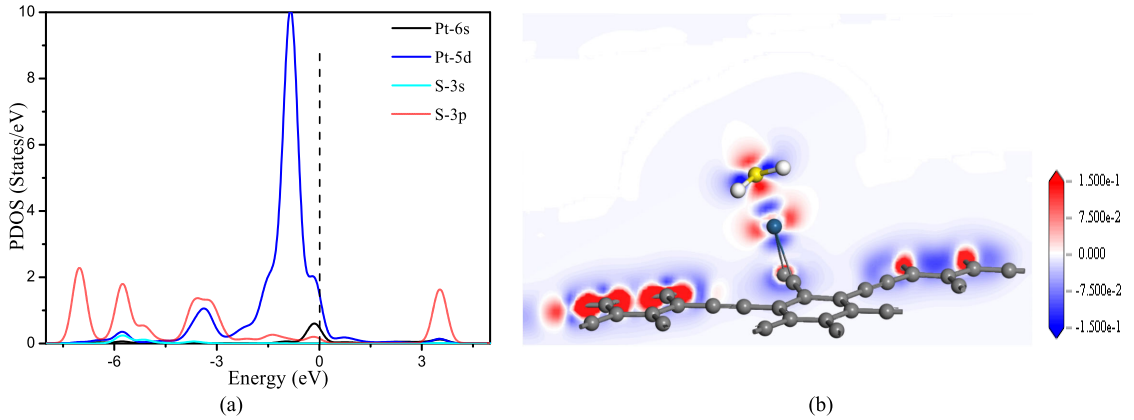

FIGURE 4. (a) PDOS of S atom and Pt atom, (b) electronic differential density map.

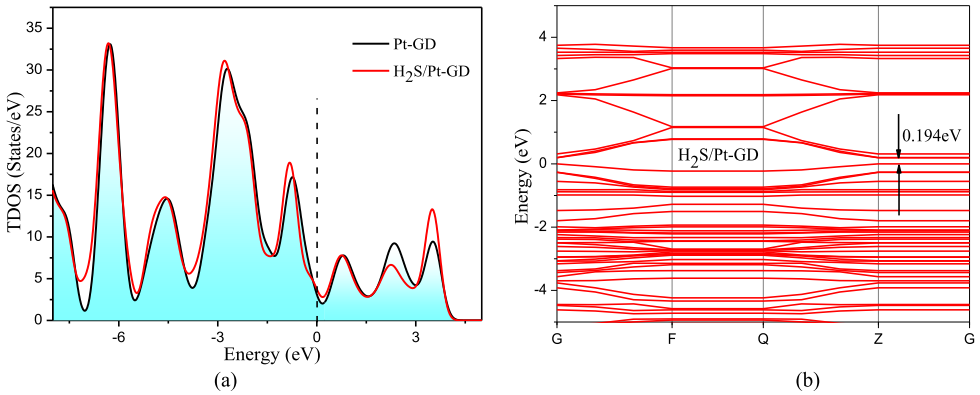

FIGURE 5. (a) TDOS of Pt-GD before and after adsorption, (b) band gap of H_2S/ Pt–GD.

of electron density in this work are indicated in red and blue, respectively. The electron density of S atom evidently increased when H atoms were considerably decreased, and the electrons of Pt preferred to assemble on the plane parallel to GD. This finding was consistent with the previous conclusion. In addition, energy gap, band gap, and the change of TDOS after adsorption are illustrated by Fig. 5 to summarize the conductivity change.

The decrease of energy gap might result in an electrical conductivity change of the monolayer according to the following expression:

$$\sigma \propto \exp(\frac{-E_g}{2kT})$$

Here, T is the temperature and k is the Boltzmann constant. Apparently, a decrease in energy band gap can exponentially change the electrical conductivity.

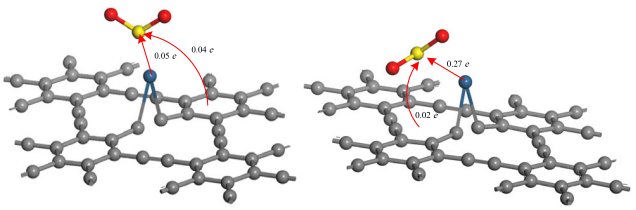

FIGURE 6. Final adsorption structures for different initial adsorption sites.

C. ADSORPTION AND GAS SENSITIVITY UPON SO_2

Fig. 6 shows the stable adsorption structure determined through the same method as that for H_2S, and the information is listed in Table 4. For the structure in Fig. 6(a), the adsorption energies were -1.13 (< -0.6 eV) and -1.24 eV (< -0.6 eV) at adsorption distances of 2.31 and 2.4 Å,

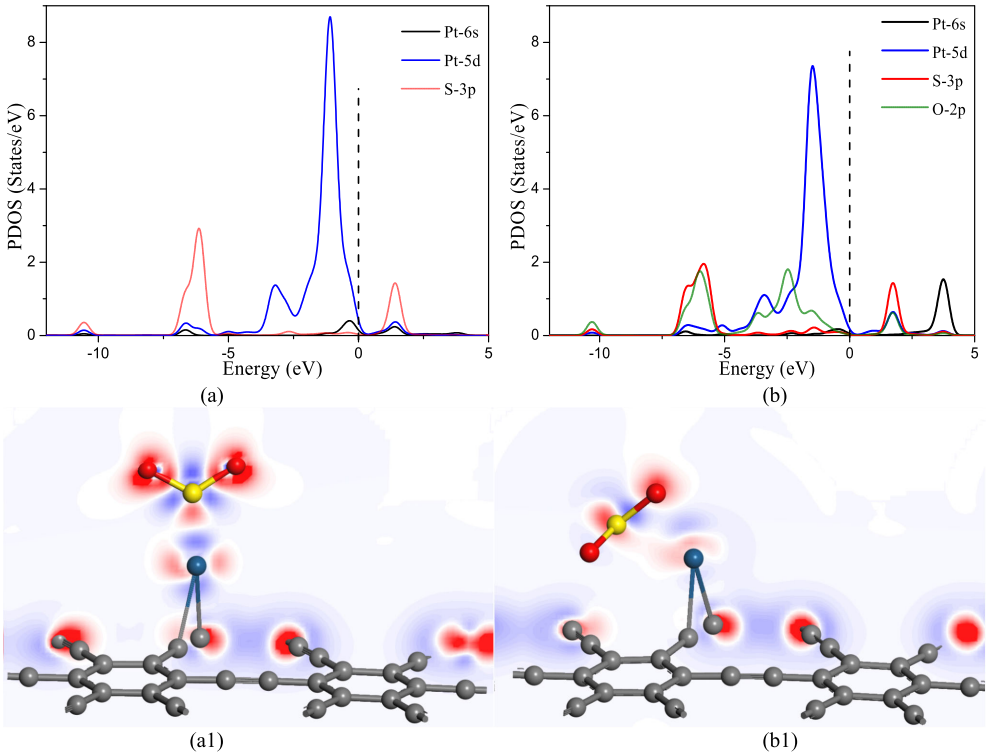

FIGURE 7. PDOS and electron deformation density maps of two adsorption results. (a) PDOS of the first adsorption configuration, (b) PDOS of the second adsorption configuration, (a1) electron deformation density map of the first adsorption configuration, (b1) electron deformation density map of the second adsorption configuration.

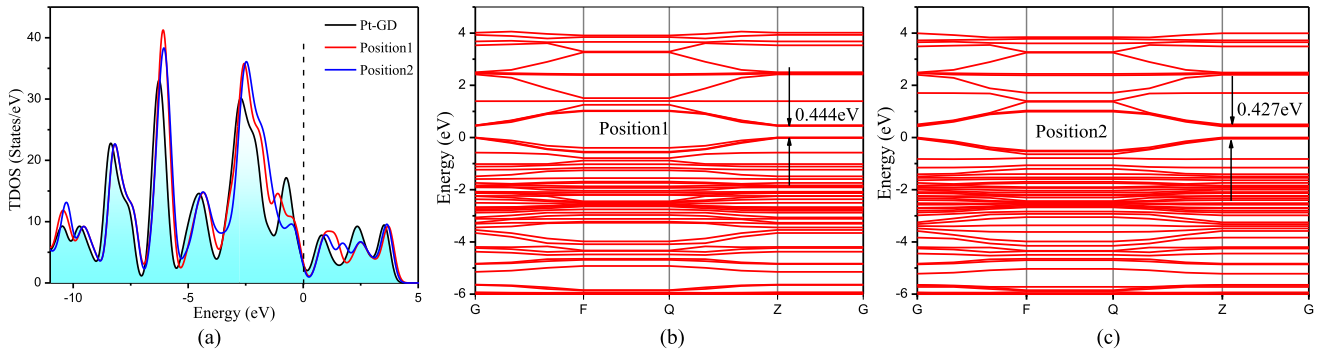

FIGURE 8. (a) TDOS curves of all adsorption sites, (b)the band gap after adsorption of position1, (b)the band gap after adsorption of position2.

TABLE 4. Adsorption data of SO_2 gas molecule.

Configuration	E_{ads} (eV)	$d_{Pt\text{-}S}$(Å)	$d_{Pt\text{-}O}$(Å)	Q (e)	E_{gap} (eV)
S	-1.13	2.31	3.30	-0.09	0.41
O	-1.24	2.45	2.35	-0.29	0.40

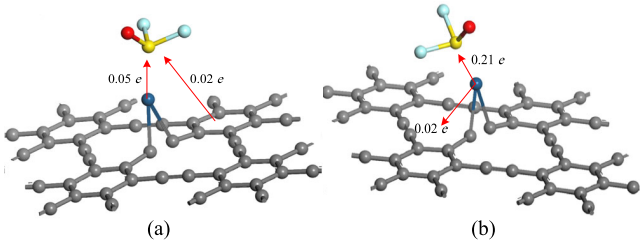

FIGURE 9. Final adsorption results of different adsorbed objects.

respectively. The quantity of the charge transferred was approximately −0.29 e, indicating a large amount of electron exchange between Pt dopant and gas molecule. Pt dopant plays a major charge contributor role. The large charge transfer may indicate a strong chemisorption between Pt dopant and SO_2 molecule.

Furthermore, we analyzed orbital hybridization after adsorption through PDOS, as shown in Fig. 7. Fig. 7(a) and (b) correspond to Fig. 6(a) and (b), respectively. The orbital

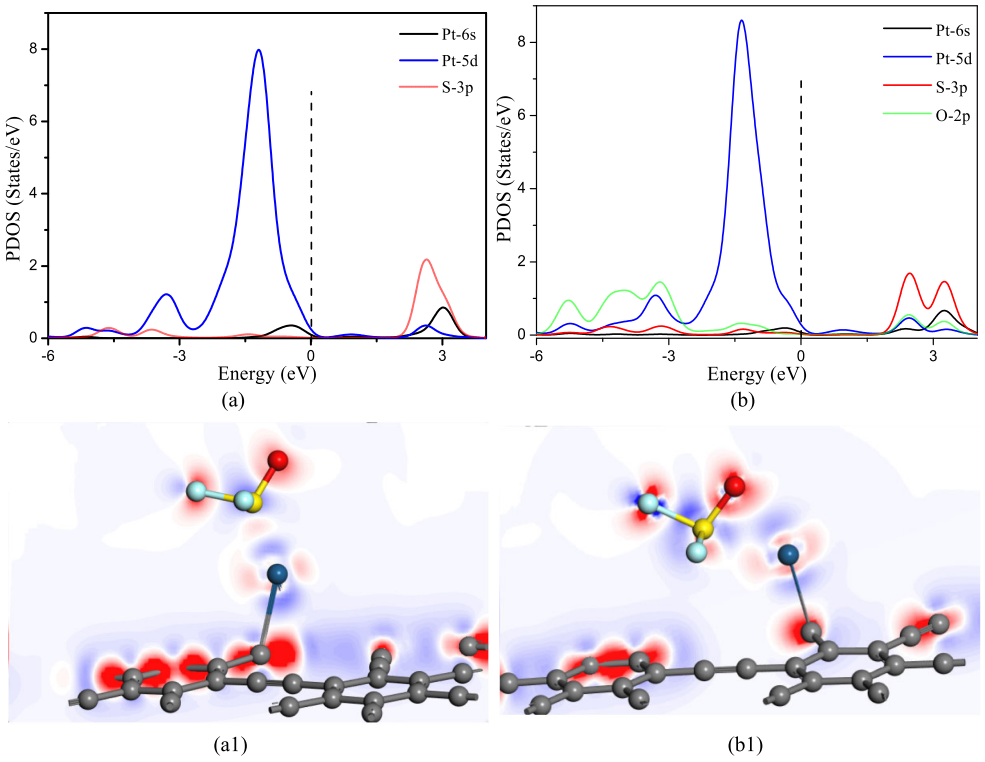

FIGURE 10. PDOS and electron deformation density maps of two adsorption results. (a) PDOS of the first adsorption configuration, (b) PDOS of the second adsorption configuration, (a1) electron deformation density map of the first adsorption configuration, (b1) electron deformation density map of the second adsorption configuration.

hybridization was not pronounced in Fig. 7(a). By contrast, hybridization occurred between Pt-5d and O-2p orbitals at the range of −5 eV to −2.5 eV, whereas S-3p, Pt-5d, and O-2p hybridization was remarkable at the range of 1.5 eV to 2.5 eV. Compared with that in Fig. 7(a), Pt-5d in Fig. 7(b) showed decreased PDOS at the range of −2 eV to 0 eV because it contributes high charge to SO_2 and orbital hybridization with O-2p. The O atoms in SO_2 played a major role in electronic reception, as shown in Fig. 7(a1) and (a2), which was consistent with the strength of the atomic electronegativity in SO_2.

Furthermore, we analyzed orbital hybridization after adsorption through PDOS, as shown in Fig. 7. Fig. 7(a) and (b) correspond to Fig. 6(a) and (b), respectively. The orbital hybridization was not pronounced in Fig. 7(a). By contrast, hybridization occurred between Pt-5d and O-2p orbitals at the range of −5 eV to −2.5 eV, whereas S-3p, Pt-5d, and O-2p hybridization was remarkable at the range of 1.5 eV to 2.5 eV. Compared with that in Fig. 7(a), Pt-5d in Fig. 7(b) showed decreased PDOS at the range of −2 eV to 0 eV because it contributes high charge to SO_2 and orbital hybridization with O-2p. The O atoms in SO_2 played a major role in electronic reception, as shown in Fig. 7(a1) and (a2), which was consistent with the strength of the atomic electronegativity in SO_2.

Fig. 8(a) shows the TDOS of Pt–GD before and after adsorption. Position1 and positon2 in Fig. 8 (a) correspond to Fig. 6 (a) and (b), respectively. The TDOS of position2 was higher than that of position1 in the energy level range near 2 eV and below −1.5 eV due to orbital hybridization between Pt and SO_2. Pt as a major charge contributor resulted in the lower TDOS of position2 than that of position1 in the other range. Both TDOS curves near the Fermi level decreased evidently after adsorption and resulted in a decrease in the conductivity of the entire structure. The band gap increased from 0.24 eV to 0.43 eV, and energy gap increased from 0.22 eV to 0.41 eV after adsorption, as shown in Fig. 8. Table 4 further indicates that the conductivity of the entire structure was weakened.

The Pt–GD monolayer is suitable for SO_2 detection because of its good adsorption properties and remarkable changes in conductivity after adsorption.

TABLE 5. Adsorption data of SOF_2 gas molecule.

configuration	E_{ads} (eV)	d (Å)	Q (e)	E_{gap} (eV)
(a)	-0.96	2.30	-0.07	0.41
(b)	-0.83	*2.47*	-0.21	0.41

D. ADSORPTION AND GAS SENSITIVITY UPON SOF_2

In this section, Fig. 9 shows two stable adsorption sites, and Table 5 shows the corresponding adsorption information. E_{ads} column in Table 5 indicates that the adsorption energy of Pt–GD upon S and O atoms was −0.96 and −0.83 eV (< −0.6 eV), respectively.

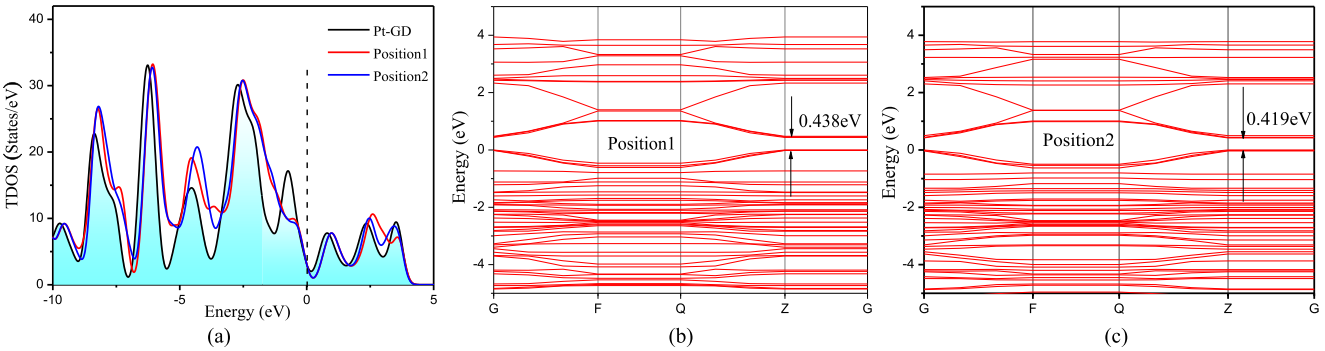

FIGURE 11. (a) TDOS curves of all adsorption sites, (b)the band gap after adsorption of position1, (b)the band gap after adsorption of position2.

TABLE 6. Adsorption data between PT–GD and SF_6 molecule.

Structure	Site	E_{ads} (eV)	d (Å)	Q (e)
Pt-GD/SF_6	*Position1*	-0.14	2.38	-0.17
	Position2	-0.10	2.75	-0.00

SOF_2 obtained numerous electrons from Pt–GD, which was mainly contributed by Pt, as shown in Fig. 9.

The PDOS and electronic differential density maps are shown in Fig. 10, and color mapping of electronic differential density maps was set from −0.4 to 0.4. Fig. 10(a1) and (b1) show the electronic differential density maps of position1 and position2, respectively. In Fig. 10(a1) and (b1), the electron density of O and F atoms was increased considerably with a decrease of S atom. The electron density of Pt's inner orbital increased, and the electron density of outer orbital, which represents higher energy level, was reduced. This result indicates that the DOS of Pt will move a distance to the left, which was proven in Fig. 10. In Fig. 10, the DOS peak of Pt-5d moved from −1 eV (Fig. 2(b)) to −1.5 eV, and orbital hybridization occurred with S-3p and O-2p.

Finally, the TDOS and band gap after adsorption are shown in Fig. 11. The DOS of position1 and position2 was smaller than that of intrinsic Pt-GD near the Fermi level because Pt contributes numerous electrons, and the band gap was increased from 0.24 eV to 0.44 eV and 0.42 eV, as shown in Fig. 11(a)–(b). The energy gap increased form 0.22 eV to 0.41 eV, and the chemisorption of Pt–GD upon SOF_2 caused a decrease in conductivity. Therefore, Pt–GD monolayer can be considered as a material with favorable adsorption properties and conductivity change upon SOF_2.

E. ADSORPTION AND GAS SENSITIVITY UPON SF_6

Table 6 shows the adsorption information of Pt-GD monolayer upon SF_6. The position1 and positon2 of Pt–GD/SF_6 represent a single F and two F atoms as the adsorbed objects, respectively. The adsorption energy (E_{ads}) of Pt-GD/SF_6 is −0.14 eV (> −0.6 eV), and the adsorption distance is 2.38 Å, which is too long to generate a chemical bond. Thus, Pt–GD monolayer can be applied in SF_6 gas because of its poor adsorption to SF_6.

IV. CONCLUSION

In this work, we investigated the possible stable structure of Pt–GD monolayer and found that the Pt dopant preferred to be adsorbed onto the C≡C bond. The Pt–GD has higher conductivity and stability than intrinsic GD monolayer. Furthermore, DFT calculation was carried out to evaluate the chemical and physical interactions between the Pt–GD and four typical gases, namely, H_2S, SO_2, SOF_2, and SF_6. Results indicated that only H_2S, SO_2, and SOF_2 molecules were adsorbed onto the Pt–GD with strong chemical interactions. The strong interactions were mainly caused by Pt atom because of its surface activity. The conductivity of monolayer was enhanced by H_2S but was weakened by SO_2 and SOF_2. The adsorption capacity occurred in the following order: SO_2 > H_2S > SOF_2 > SF_6.

The targeted adsorption and conductivity changes of Pt–GD to SF_6 decomposition products in SF_6 gas indicated that Pt–GD is a novel material that is suitable for the detection of SF_6 decomposition products. This calculation provides theoretical support for a novel material realizing the operation state evaluation of SF_6 insulated gas equipment.

REFERENCES

[1] S. Yanabu, Y. Murayama, and S. Matsumoto, "SF_6 insulation and its application to HV equipment," *IEEE Trans. Elect. Insul.*, vol. 26, no. 3, pp. 358–366, Jun. 1991.

[2] F. Y. Chu, "SF_6 decomposition in gas-insulated equipment," *IEEE Trans. Elect. Insul.*, vol. EI-21, no. 5, pp. 693–725, Oct. 1986.

[3] M. Evans, C. W. Hsu, P. Heimann, and C. Y. Ng, "A high resolution energy-selected kinetic energy release study of the process $SF_6+h\nu SF_5^+ + F + e^-$: Heat of formation of SF_5+," *J. Chem. Phys.*, vol. 106, no. 3, pp. 978–981, 1997.

[4] I. Sauers, "Evidence for SF_4 and SF_2 formation in SF_6 corona discharges," presented at the Elect. Insul. Dielectric Phenomena Conf., Oct. 1991.

[5] Y. Fu, A. Yang, X. Wang, A. B. Murphy, X. Li, D. Liu, Y. Wu, and M. Rong, "Theoretical study of the neutral decomposition of SF_6 in the presence of H_2O and O_2 in discharges in power equipment," *J. Phys. D-Appl. Phys.*, vol. 49, no. 38, Aug. 2016, Art. no. 385203.

[6] J. Tang, F. Liu, X. Zhang, Q. Meng, and J. Zhou, "Partial discharge recognition through an analysis of SF_6 decomposition products part 1: Decomposition characteristics of SF 6 under four different partial discharges," *IEEE Trans. Dielectr. Elect. Insul.*, vol. 19, no. 1, pp. 29–36, Feb. 2012.

[7] Y. Qiu, J. Yuan, and X. Chen, "Influence of trace impurities from SF_6 new gas on the life of SF_6-insulating electrical equipment," *High Voltage Eng.*, vol. 39, no. 2, pp. 360–364, 2013.

[8] Y. Li, L. Xu, H. Liu, and Y. Li, "Graphdiyne and graphyne: From theoretical predictions to practical construction," *Chem. Soc. Rev.*, vol. 43, no. 8, pp. 2572–2586, 2014.
[9] G. Li, Y. Li, H. Liu, Y. Guo, Y. Li, and D. Zhu, "Architecture of graphdiyne nanoscale films," *Chem. Commun.*, vol. 46, pp. 3256–3258, Jan. 2010.
[10] X. Qian, H. Liu, C. Huang, S. Chen, L. Zhang, Y. Li, J. Wang, and Y. Li, "Self-catalyzed growth of large-area nanofilms of two-dimensional carbon," *Sci. Rep.*, vol. 5, Jan. 2015, Art. no. 7756.
[11] R. Lu, D. Rao, Z. Lu, J. Qian, F. Li, H. Wu, Y. Wang, C. Xiao, K. Deng, E. Kan, and W. Deng, "Prominently improved hydrogen purification and dispersive metal binding for hydrogen storage by substitutional doping in porous graphene," *J. Phys. Chem. C*, vol. 116, no. 40, pp. 21291–21296, Sep. 2012.
[12] Z. Jia, Y. Li, Z. Zuo, H. Liu, C. Huang, and Y. Li, "Synthesis and properties of 2D carbon-graphdiyne," *ACC Chem. Res.*, vol. 50, no. 10, pp. 2470–2478, Oct. 2017.
[13] S. W. Cranford and M. J. Buehler, "Selective hydrogen purification through graphdiyne under ambient temperature and pressure," *Nanoscale*, vol. 4, no. 15, p. 4587, 2012.
[14] H. Zhang, Y. Xia, H. Bu, X. Wang, M. Zhang, Y. Luo, and M. Zhao, "Graphdiyne: A promising anode material for lithium ion batteries with high capacity and rate capability," *J. Appl. Phys.*, vol. 113, no. 4, Jan. 2013, Art. no. 044309.
[15] Y. Li, X. Li, Y. Meng, and X. Hun, "Photoelectrochemical platform for MicroRNA let-7a detection based on graphdiyne loaded with AuNPs modified electrode coupled with alkaline phosphatase," *Biosens. Bioelectron.*, vol. 130, pp. 269–275, Apr. 2019.
[16] V. Nagarajan and R. Chandiramouli, "Investigation of NH_3 adsorption behavior on graphdiyne nanosheet and nanotubes: A first-principles study," *J. Mol. Liquids*, vol. 249, pp. 24–32, Jan. 2018.
[17] V. Nagarajan, U. Srimathi, and R. Chandiramouli, "First-principles insights on detection of dimethyl amine and trimethyl amine vapors using graphdiyne nanosheets," *Comput. Theor. Chem.*, vol. 1123, pp. 119–127, Jan. 2018.
[18] Z. Meng, X. Zhang, Y. Zhang, H. Gao, Y. Wang, Q. Shi, D. Rao, Y. Liu, K. Deng, and R. Lu, "Graphdiyne as a high-efficiency membrane for separating oxygen from harmful gases: A first-principles study," *ACS Appl. Mater. Interfaces*, vol. 8, no. 41, pp. 28166–28170, Oct. 2016.
[19] X.-Y. Liu, J.-M. Zhang, K.-W. Xu, and V. Ji, "Improving SO_2 gas sensing properties of graphene by introducing dopant and defect: A first-principles study," *Appl. Surf. Sci.*, vol. 313, pp. 405–410, Sep. 2014.
[20] S. Kim and J. Y. Lee, "Doping and vacancy effects of graphyne on SO_2 adsorption," *J. Colloid Interface Sci.*, vol. 493, pp. 123–129, May 2017.
[21] B. Huang, Z. Li, Z. Liu, G. Zhou, S. Hao, J. Wu, B.-L. Gu, and W. Duan, "Adsorption of gas molecules on graphene nanoribbons and its implication for nanoscale molecule sensor," *J. Phys. Chem. C*, vol. 112, pp. 13442–13446, Aug. 2008.
[22] M. Zhou, Y.-H. Lu, Y.-Q. Cai, C. Zhang, and Y.-P. Feng, "Adsorption of gas molecules on transition metal embedded graphene: A search for high-performance graphene-based catalysts and gas sensors," *Nanotechnology*, vol. 22, no. 38, Aug. 2011, Art. no. 385502.
[23] S. Chen and Z. Xi, "Modulation of molecular sensing properties of graphdiyne based on 3D impurities," *Acta Phys.-Chim. Sinica*, vol. 34, no. 9, pp. 1061–1073, Apr. 2018.
[24] A. A. Peyghan, S. F. Rastegar, and N. L. Hadiwpour, "DFT study of NH_3 adsorption on pristine, Ni- Si-doped graphynes," *Phys. Lett. A*, vol. 378, nos. 30–31, pp. 2184–2190, Jun. 2014.
[25] J. Beheshtian, A. A. Peyghan, Z. Bagheri, and M. B. Tabar, "Density-functional calculations of HCN adsorption on the pristine and Si-doped graphynes," *Struct. Chem.*, vol. 25, no. 1, pp. 1–7, Feb. 2014.
[26] Z. Lu, L. Peng, D. Ma, X. Yang, S. Li, and Z. Yang, "Detection of gas molecules on single Mn adatom adsorbed graphyne: A DFT-D study," *J. Phys. D Appl. Phys.*, vol. 51 , no. 6, Jan. 2018, Art. no. 065109.
[27] A. Seif, M. J. López, A. Granja-Delrío, K. Azizi, and J. A. Alonso, "Adsorption and growth of palladium clusters on graphdiyne," *Phys. Chem. Chem. Phys.*, vol. 19, no. 29, pp. 19094–19102, 2017.
[28] S. Kim, A. R. Puigdollers, P. Gamallo, F. Viñes, and Y. L. Jin, "Functionalization of γ-graphyne by transition metal adatoms," *Carbon*, vol. 120, pp. 63–70, Aug. 2017.
[29] G. Javahery, S. Petrie, J. Wang, and D. K. Bohme, "A theoretical study on the cyclopropane adsorption onto the copper surfaces by density functional theory and quantum chemical molecular dynamics methods," *J. Mol. Catal. A, Chem.*, vol. 220, no. 2, pp. 189–198, Oct. 2004.
[30] J. P. Perdew, K. Burke, and M. Ernzerhof, "Generalized gradient approximation made simple," *Phys. Rev. Lett.*, vol. 77, pp. 3865–3868, Oct. 1996.
[31] D. W. Ma, T. Li, Q. Wang, G. Yang, C. He, B. Ma, and Z. Lu, "Graphyne as a promising substrate for the noble-metal single-atom catalysts," *Carbon*, vol. 95, pp. 756–765, Dec. 2015.
[32] D. J. Chadi, ""Special points for Brillouin-zone integrations"—A reply," *Phys. Rev. B, Condens. Matter*, vol. 16, no. 4, pp. 1746–1747, Aug. 1977.

YINGANG GUI was born in Chongqing, China, in 1988. He received the B.Sc. degree in applied physics from Chongqing Normal University, in 2011 and the Ph.D. degree in electrical engineering from Chongqing University, in 2017. He has been rewarded the Chinese Government Scholarship to sponsor the joint training program as a Ph.D. in the Georgia Institute of Technology, USA. He is currently a Lecturer with the Department of Electrical Engineering, College of Engineering and Technology, Southwest University, China. He studies high-voltage electric equipment insulation online monitoring and fault diagnosis.

XIN HE was born in Guangan, Sichuan, China, in 1996. He received the B.S. degree in automation from Southwest University, China, in 2017, where he is currently pursuing the M.S. degree with the College of Engineering Technology. His research interests include high-voltage electric equipment insulation online monitoring and fault diagnosis.

ZHUYU DING was born in Dianjing, Chongqing, China. He received the B.Sc. degree in computer science and technology and the M.Sc. degree in agricultural mechanization engineering from Southwest University, China, in 2005 and 2009, respectively, where he is currently an Associate Professor with the College of Engineering Technology. His main research interests include agricultural mechanization and mechatronics.

CHAO TANG was born in Sichuan, China, in 1981. He received the M.S. and Ph.D. degrees in electrical engineering from Chongqing University, China, in 2007 and 2010, respectively. As a Ph.D. Student, from 2008 to 2009, and as a Visiting Scholar, in 2013 and from 2015 to 2016, he was with the Tony Davies High Voltage Lab, University of Southampton, U.K., doing some researches on the dielectric response characteristics and space charge behaviors of oil-paper insulation. He is currently a Professor with the College of Engineering Technology, Southwest University, China. His research interests include on-line monitoring of insulation conditions and fault diagnosis for high-voltage equipment.

LINGNA XU received the B.Sc. degree from the University of Science and Technology Beijing, in 2008, the M.Sc. degree from the Polytechnic Institute of New York University, in 2010, and the Ph.D. degree in electrical engineering from Chongqing University. She is currently a Lecturer with the Department of Electrical Engineering, College of Engineering and Technology, Southwest University. Her main research interests include online monitoring and fault diagnosis of power equipment, condition-based maintenance, and the internal insulation and thermal properties of power transformers.